Biomaterials 301 (2023) 122246

Contents lists available at ScienceDirect

Biomaterials

journal homepage: www.elsevier.com/locate/biomaterials

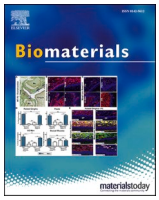

Hydrogel-encapsulation to enhance bacterial diagnosis of colon inflammation

Samira Aghlara-Fotovat [a,1], Elena Musteata [b,1], Michael D. Doerfert [a], Moshe Baruch [a], Maya Levitan [a], Jeffrey J. Tabor [a,b,c,**], Omid Veiseh [a,*]

[a] Department of Bioengineering, Rice University, Houston, TX, USA
[b] Systems Synthetic and Physical Biology, Rice University, Houston, TX, USA
[c] Department of Biosciences, Rice University, Houston, TX, USA

ARTICLE INFO

Keywords:
Hydrogel encapsulation
Synthetic biology
Diagnostic bacteria
Colitis

ABSTRACT

Bacteria can be genetically programmed to sense and report the presence of disease biomarkers in the gastrointestinal (GI) tract. However, diagnostic bacteria are typically delivered via oral administration of liquid cultures, resulting in poor survival and high dispersal *in vivo*. These limitations confound recovery and analysis of engineered bacteria from GI or stool samples. Here, we demonstrate that encapsulating bacteria inside of alginate core-shell particles enables robust survival, containment, and diagnostic function *in vivo*. We demonstrate these benefits by encapsulating a strain engineered to report the presence of the biomarker thiosulfate via fluorescent protein expression in order to diagnose dextran sodium sulfate-induced colitis in rats. Hydrogel-encapsulated bacteria engineered to sense and respond to physiological stimuli should enable minimally invasive monitoring of a wide range of diseases and have applications as next-generation smart therapeutics.

1. Introduction

The human GI tract harbors trillions of bacteria comprising over 500 species [1,2]. Core physiological processes such as metabolism, immune-, and brain function are affected by interactions between gut microbes and the host [3–7]. Disruption of gut bacterial-host interactions are linked to obesity, type 2 diabetes, hepatic steatosis, inflammatory bowel disease (IBD), and several types of cancer [8,9]. Thus, gut metabolites and signaling molecules could serve as biomarkers of a wide range of diseases [10–13].

Genetically engineered bacteria have potential to sense and report gut biomarkers in order to diagnose diseases [14–19]. For example, we recently discovered a thiosulfate ($S_2O_3^{2-}$)-activated two-component regulatory system we named ThsSR in the marine bacterium *Shewanella halifaxensis* and repurposed it to program the human probiotic E. *coli* Nissle 1917 (hereafter Nissle) to diagnose dextran sodium sulfate (DSS)-induced colitis in mice [20]. ThsSR comprises the membrane-bound sensor kinase ThsS and the cytoplasmic response regulator ThsR. In the presence of extracellular thiosulfate, ThsS phosphorylates ThsR, which then induces transcription from the P_{phsA} target promoter. To diagnose colitis, we expressed ThsSR in Nissle and utilized superfolder green fluorescent protein (sfGFP) expression to monitor P_{phsA} activity. We further engineered this strain to constitutively express the red fluorescent protein mCherry, enabling us to identify it within complex GI and stool samples. Using flow cytometry, we observed a clear relationship between the extent of colon inflammation and ThsSR activity [20]. Using a similar approach, we utilized an acidic pH-sensing TCS to engineer *E. coli* to report ileal inflammation in a mouse genetic model of Crohn's Disease [21]. In other work, *E. coli* engineered to express GFP from a fucose-activated promoter were used to measure fucose liberated by the gut commensal *B. acidifaciens* from the mouse intestine [22]. The human commensal bacterium *B. thetaiotaomicron* has been engineered to sense and respond to exogenous rhamnose and arabinogalactan supplemented by diet to the murine gut [23]. Finally, a tetrathionate sensing two-component regulatory system from *S. typhimurium* was combined with an engineered genetic memory device to engineer *E. coli* to report inflammation in both infection-induced and genetic mouse models [24].

* Corresponding author.
** Corresponding author. Department of Bioengineering, Rice University, Houston, TX, USA.
E-mail addresses: jeff.tabor@rice.edu (J.J. Tabor), omid.veiseh@rice.edu (O. Veiseh).
[1] These authors contributed equally to this work.

https://doi.org/10.1016/j.biomaterials.2023.122246
Received 19 January 2023; Received in revised form 13 June 2023; Accepted 12 July 2023
Available online 12 July 2023

Despite these early advances, delivery of engineered bacteria to the gut environment remains a challenge [25,26]. In particular, liquid cultures of engineered bacteria are typically delivered orally or to the stomach via gavage. Administered bacteria may encounter the envelope-destroying enzyme lysozyme in the mouth [27], a highly acidic pH in the mammalian stomach [28,29], and antimicrobial bile salts in the small intestine [30,31], greatly reducing their viability. Furthermore, the administered bacterial bolus disperses throughout the GI tract, which can exacerbate low bacterial recovery from stool for analysis [20,21]. Techniques to enhance survival and containment in the GI tract could broaden the applications of engineered bacteria in the gut environment.

In biomedical engineering, hydrogel encapsulation is commonly used to deliver cells of interest to target *in vivo* tissues [32]. Biomaterial carriers can provide a protective, semi-controllable environment to support the growth and viability of encapsulated cells. In particular, marine polysaccharides such as alginate have garnered attention due to their cost-efficiency and widespread availability, as well as their cytocompatibility, which enables their use with versatile cell types [33]. Furthermore, alginate can be polymerized via mild ionic crosslinking reactions to provide a semi-permeable barrier for the containment of live cells, enabling them to transmit or receive signals from their surroundings. The gels formed through this process exhibit advantageous physicochemical properties including water insolubility, pH responsiveness, and tunable mechanical strength. Encapsulation has also been used by the food industry to enhance delivery of probiotics to the gut [34–36]. Various studies have demonstrated that bacterial encapsulation within alginate polymers can improve viability in simulated gastric and intestinal fluid [37].

Due to these advantages, researchers have begun to encapsulate bacteria for therapeutic applications. In early work, Prakash *et al.* used alginate-poly-L-lysine-alginate (APA) to encapsulate *E. coli* genetically engineered to express the enzyme urease. They then demonstrated that oral administration of these encapsulated microbes helps maintain normal plasma urea levels in uremic rats [38]. In other work, alginate was used to encapsulate a microbial community of *E. coli, B. coagulans*, and *E. hormaechei* strains isolated from mouse fecal samples for their ability to metabolize urea and creatinine into amino acids [39]. This encapsulated microbial consortium was used to clear metabolic wastes and treat kidney failure in murine and porcine models [39]. Other probiotic strains, such as *L. salivarius*, have been delivered via encapsulation in chitosan-alginate gels to improve disease outcome in mice with DSS-induced colitis [40]. More recently, Yang *et al.* engineered *E. coli* and *L. lactis* to produce interferon gamma (IFN-γ) and transforming growth factor beta-1 (TGF-β 1), respectively, in response to optogenetic stimulation. They subsequently encapsulated these strains in a chitosan-sodium alginate polymer to improve bacterial colonization in the mouse gut [41]. Dai *et al.* used chitosan and alginate microcapsules to confine engineered bacteria and achieve cell density-dependent lysis that releases protein products in a programmable way responsive to cell-material feedback [42]. As a final example, Han *et al.* developed chitosan microcapsules for the subcutaneous administration of bacteria engineered to produce protein drugs [43]. While such systems have been successful in releasing therapeutics or responding to co-administered stimuli such as light or small molecule inducers, they have not often been used to directly monitor physiological signals or diagnose disease. Additionally, the probiotic delivery systems developed to date have been tested primarily on *in vitro* digestion models that are unable to accurately simulate the animal GI tract [37]. To our knowledge, no previous research has directly measured the survival of encapsulated bacteria in a mammalian model.

Here, we utilize alginate polymer encapsulation to improve the delivery and recovery of engineered colitis-sensing bacteria in a rat model (Fig. 1). Specifically, we encapsulate our previous thiosulfate-sensing Nissle strain into millimeter-scale hydrogels using electrostatic spraying. We develop mechanical processing methods to physically release bacteria from the hydrogels for downstream analysis via flow cytometry. By quantifying live cell numbers before and after encapsulation, we demonstrate that the encapsulation process is non-toxic. We then show encapsulation protects bacteria from death at pH = 3.2, the pH of the rat stomach [44]. We go on to deliver 10^7 encapsulated thiosulfate-sensing bacteria to rats prior to and following DSS treatment and recover them from stool. Selective plating reveals that our bacteria increase in numbers during GI transit, in stark contrast to the far lower numbers previously recovered without encapsulation. We also show that the hydrogel capsules maintain morphological integrity *in vivo*. We assess the fluorescent reporter activation of retrieved bacteria via flow cytometry and confirm that ThsSR is activated by DSS-induced gut inflammation in all animals. Finally, we demonstrate that reporter fluorescence correlates with animal disease state as measured by disease activity index (DAI), suggesting that our encapsulated bacterial biosensors can accurately diagnose gut inflammation *in vivo*.

2. Materials and methods

2.1. DNA and bacterial strains

Wild-type *E. coli* Nissle 1917 (gift from the Sebastian Winter group) was used for viability staining experiments. Strain KD01, an engineered thiosulfate-sensing *E. coli* Nissle 1917 strain resistant to

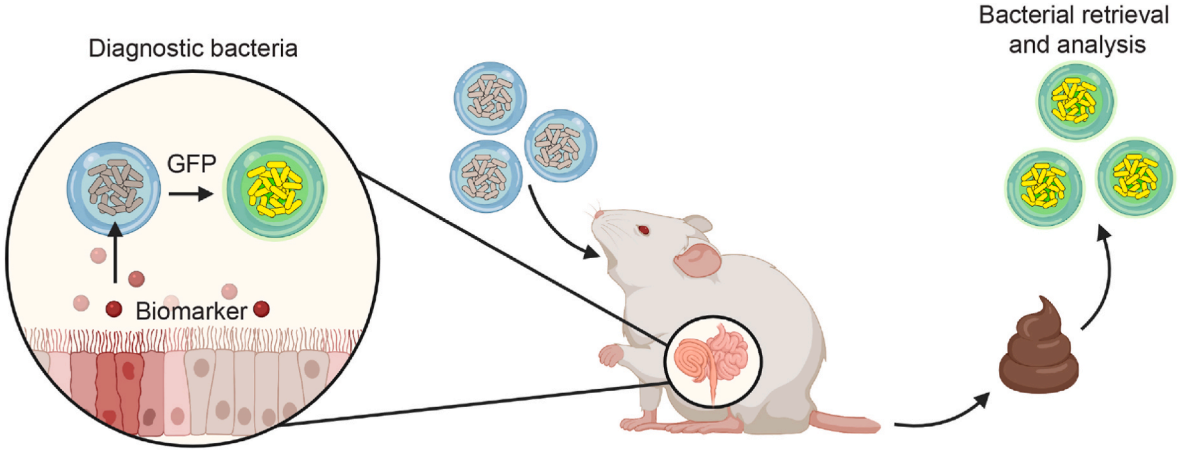

Fig. 1. Delivery of alginate-encapsulated diagnostic bacteria to the gut. Engineered bacteria are encapsulated and administered orally. Small molecule biomarkers diffuse through the capsules, activating the expression of a bacterial reporter gene. The capsules are recovered from stool or GI tissue sites for downstream analysis.

chloramphenicol and spectinomycin [20], was used for all other bacterial experiments. Freezer aliquots of KD01 were prepared by growing a colony in LB Miller broth and the appropriate antibiotics (35 μg/ml chloramphenicol and 100 μg/mL spectinomycin) to OD_{600}–0.5, adding glycerol to a 15% v/v final concentration, and freezing at −80 °C. All experiments were performed aerobically.

2.2. Bacterial preparation for encapsulation

Overnight cultures were started from freezer stocks in LB with the appropriate antibiotics and incubated shaking for 18 h at 250 rpm at 37 °C. Cultures were then diluted 100X into fresh LB with appropriate antibiotics and incubated shaking at 250 rpm at 37 °C to OD600–0.1. Cultures were placed on ice to stop cell growth, and the remaining procedure was performed on ice or at 4 °C. Cultures were transferred into sterile, ice-cold tubes and centrifuged at 4000 g for 10 min. Cells were washed once with sterile, ice-cold PBS, to remove traces of LB. Cells were then concentrated 10X into a 1:19 solution of PBS:alginate (1.4% wt/vl PRONOVA SLG20 alginate, Novamatrix Product #4202001, diluted in 0.8% saline). The resulting bacterial alginate suspension was used as the core solution for the encapsulation procedure. All capsules prepared in this work were formed with a core-shell structure where bacteria are loaded only into the core, with an average core radius of 450 μm, such that the capsule core volume is ~0.38 μL. For free cell experiments, the cells were concentrated into a 1:19 solution of PBS:LB rather than PBS:alginate, and 1.9 μL of the resulting bacterial suspension was used to model the bacterial load of 5 capsules.

2.3. Bacterial encapsulation within alginate hydrogels

The bacterial alginate suspension was prepared as described and loaded into a 5 mL Luerlock syringe to be used for the capsule core. Another identical syringe was loaded with SLG20 alginate to be used for the capsule shell. Alginate hydrogel capsules were synthesized using a custom-built, two-fluid co-axial electrostatic spraying device. The device consists of a voltage generator (Gamma High Voltage, 1-ES10N–5W) attached to the tip of a co-axial needle (Rame-Hart Instrument Co., 10-10-COAXIAL-2218) and grounded to a 1:4 $BaCl_2$:mannitol crosslinking bath. The co-axial needle is fed by the 2 syringes described, which are placed in 2 separate syringe pumps (Harvard Apparatus, CAT#704504) and suspended over 150 mL of the crosslinking bath. For this work, the ratio between the flow rates of the core and shell syringe was set to 5:14 for a shell thickness of ~0.30 mm. Capsules drop into the crosslinking bath as they are synthesized, and incubate for 15 min. The crosslinking bath is then decanted, and capsules are washed 3X with HEPES buffer.

2.4. Dextran diffusion assays for permeability

Capsule permeability was assayed as described previously [45]. In summary, alginate solutions were prepared as described above (1.4 wt% in 0.8% saline). Saturated stock solutions of four different molecular weights of FITC-dextran were prepared (40 kDa (FD40S, Sigma), 150 kDa (FD150S, Sigma), 500 kDa (FD500S, Sigma) and 2 MDa (FD2000S, Sigma). Capsules were made for each combination of FITC-dextran and alginate by mixing 950 μl of the alginate solution with 50 μl of the FITC-dextran and then electrospraying into a barium chloride crosslinker. The capsules were crosslinked for 15 min, washed twice with HEPES buffer and then placed in Krebs buffer on ice to minimize diffusion until all groups were prepared.

After washing, five capsules were aliquoted into each well of 96-well plate, rinsed once with Krebs buffer, and then incubated in 150 μl of Krebs buffer for the duration of the study. For each time point (15 min, 1, 3, 7, and 24 h), 5 replicates were prepared for each capsule group. The plates were covered with aluminum foil to protect from light and shaken on a plate shaker at 300 r.p.m. At the indicated timepoints 50 μl of the incubation buffer was collected and transferred to a black 96-well plate. Fluorescence in each well was measured with a Tecan Infinite M Plex plate reader. Percent retention of FITC was calculated by normalizing to the theoretical maximum amount of FITC diffusion (using the diameter of the core, and the known loading concentration). At each timepoint, the percentage was calculated as one minus percent released.

2.5. Bacterial viability staining

Staining was performed according to the manufacturer's guidelines using the LIVE/DEAD® BacLight™ Bacterial viability kit (Thermo Fisher), with the following modifications to enable assaying encapsulated cells. Staining of the encapsulated cells was performed as follows: 10 capsules per replicate were washed 3X with sterile 0.9% saline, placed in 1 mL saline, and incubated on ice for 40 min. 5 capsules from each replicate were removed and processed as described below to determine the living bacterial concentration (CFU). The remaining 5 capsules were placed into 200 μL saline. The remaining procedure was performed according to vendor instructions, with the following modifications: the live/dead staining solutions were dissolved in saline, and the capsules were washed 3X with 1 mL saline prior to imaging due to high stain absorption by the alginate. The nonliving bacteria were heat-inactivated by incubation in a water bath at 65–70 °C for 40 min prior to encapsulation and staining. In parallel, equivalent amounts of free cells were prepared and stained according to the manufacturer's guidelines in order to test each stain (STYO-9 and Propidium Iodide) independently as an assay control.

2.6. Capsule microscopy

Prior to imaging, capsules were washed 3X and transferred into ~5 mL capsule buffer within a 6-well plate. Dark- and bright-field microscopy was performed using an EVOS at 2X magnification. Fluorescent microscopy images were obtained using an EVOS XL at 10X magnification. For SYTO-9 fluorescence, an excitation/emission wavelength of 480 nm/500 nm was used, and 490 nm/635 nm for propidium iodide and mCherry fluorescence. Images in this work are representative of 3 replicates for *in vitro* bacterial experiments and 10 replicates for *in vivo* rat experiments.

2.7. Hydrogel capsule processing to release bacteria

Capsules were first processed to release encapsulated bacteria and enable measurements. Each experimental condition was performed in triplicate. This procedure was performed on ice or at 4 °C. For each replicate, 5 capsules were transferred in PBS to sterile round-bottom tubes. Only 3 samples were processed at a time, to avoid cell overexposure to chelating agents. All PBS was aspirated from the capsules and replaced with 500 μL of 50 mM EDTA (pH 8). Capsules were then homogenized using an electric homogenizer blade (Fisherbrand 150 Handheld Homogenizer) at speed 3 for 10–20 s until no visible capsule fragments remain (henceforth, the homogenized capsule sample). The homogenizer blade is sterilized with 70% EtOH and washed with sterile water in between samples. Biosensing and viability assays using the homogenized sample were performed immediately following this processing procedure.

2.8. Bacterial viability assays for free and encapsulated cells

To determine the viable bacterial capsule load, the homogenized capsule sample was vortexed at speed 6 (Scientific Industries, Vortex-Genie 2) and immediately diluted 20X into PBS. Serial dilutions of the homogenized capsule sample were prepared in PBS and plated onto LB agar with appropriate antibiotics and incubated at 37 °C for ~18 h. For free cells, equal amounts of bacteria were treated similarly with EDTA

(as described in Methods 2.7) and diluted in PBS as for the capsule samples. Bacterial colonies were counted to determine the concentration (CFU/mL) of the homogenized capsule sample and to calculate the bacterial capsule load (CFU/capsule).

2.9. Bacterial recovery from stool for free and encapsulated cells

Bacteria were recovered from rat stool as described previously [24]. Briefly, fecal samples were homogenized at 100 mg/mL in sterile PBS for ~5 min. Large debris was pelleted by centrifugation at 4*g* for 20min, and serial dilutions of the resulting supernatant were cultured on selective agar plates for enumeration by colony counting. Each rat fecal pellet was weighed in order to normalize the total bacterial recovery per milligram of stool. Capsules were recovered from rat stool by dissolving the fecal pellet in PBS. Capsules were stored in PBS on ice until analysis. All capsules were collected and enumerated from each fecal pellet, and 5 were processed to release the encapsulated bacteria (Methods 2.7). The mean bacterial population of the n = 5 capsules was used to obtain the total number of bacteria in the pellet, based on the total number of capsules present in the pellet.

2.10. Bacterial biosensing assays

To determine the response of the biosensing bacteria to thiosulfate, bacteria were first encapsulated as described. Five capsules in capsule buffer were then aliquoted into wells in a sterile 96-well plate. Capsule buffer was aspirated from each well and replaced with 200 μL of M9 + glycerol (1X M9 salts, 0.4% v/v glycerol, 0.2% casamino acids, 2 mM $MgSO_4$, and 100 μM $CaCl_2$) at varying concentrations of sodium thiosulfate pentahydrate (Sigma Aldrich). For free cell experiments, bacterial suspensions were prepared as described to model the bacterial alginate suspension, and 1.9 μL of bacterial suspension was used to inoculate each well. The 96-well plate was incubated stationary at 37 °C for 6 h and then placed in an ice water bath to stop cell growth. The remaining procedure was performed on ice or at 4 °C. Capsules were processed as described. The homogenized samples were passed through Bel-Art SP Scienceware Flowmi 40 μm cell strainers (Fisher Scientific) to remove solids. The filtered samples were then diluted 10X into PBS +1 mg/ml chloramphenicol and incubated for 15 min at 37C prior to flow cytometry analysis. For free cell experiments, 1.9 μL of the final experimental culture was added to 500 μL EDTA and diluted into PBS +1 mg/ml chloramphenicol as for the capsule samples. Reported fluorescence values are not corrected for cellular autofluorescence.

2.11. Flow cytometry and data analysis

Flow cytometry analysis was performed on a BD FACScan flow cytometer with a blue (488 nm, 30 mW) and yellow (561 nm, 50 mW) laser. Fluorescence was measured on two channels: FL1 with a 510/20-nm emission filter (sfGFP), and FL3 with a 650-nm long-pass filter (mCherry). For data acquisition, events were thresholded by an SSC scatter profile characteristic of *E. coli* Nissle 1917. Cells were further thresholded in the FL3 channel, to ignore counts with low mCherry-like fluorescence. These non-fluorescent counts include alginate microfragments remaining after capsule homogenization, and native microflora from the rat GI tract. Typical event rates were between 1000 and 2000 events per second for a total of 20,000 events within the gated population. For *in vivo* experiments, data were collected for 5 min or for 20,000 counts within the gated population, whichever came first. Calibration particles (Spherotech, catalog RCP-30-20A) were run at the end of every experiment at the same photomultiplier tube voltage gain settings used for data collection. Following data acquisition, raw data were processed using FlowCal [46]. First, a standard curve was generated from the calibration beads to convert arbitrary units from the cytometer into absolute fluorescence units (MEFL for FL1 and MECY for FL3). Counts with an mCherry fluorescence value lower than 5000 MECY were discarded in order to discriminate between engineered bacteria and alginate micro-fragments or native stool microflora. Remaining counts were gated by an FSC/SSC scatter profile characteristic of *E. coli* Nissle 1917. Density gating was applied to retain 50% of the events in the densest region and isolate the main population. This data analysis pipeline is summarized visually in Fig. S4. Samples giving fewer than 250 counts by these gating procedures were discarded. Overall, capsules retrieved from DSS-treated rats gave more counts/sample than those retrieved from rats prior to DSS treatment.

2.12. Dextran sodium sulfate rat experiments

All animal studies were performed in accordance with guidelines established by the Animal Welfare Committee. Sprague Dawley rats were weighed on day 0, prior to any manipulation. Stool was collected and checked for occult blood (Thermo Fisher, Hemoccult 60151). Capsules were administered via oral gavage (Instech, FTPU-13-88-50) and retrieved from stool samples of healthy rats at this stage. To establish intestinal inflammation, rats were provided drinking water with 3–5% wt/v dextran sulfate sodium for 12 days (Thermo Fisher, J63606.22). The body weight, stool consistency and presence of gross bleeding or occult blood in feces for each animal were scored daily from 0 to 4. The score in each category was summed to determine the animals overall disease activity index (DAI); no weight loss, normal stool consistency, negative hemoccult: 0; 1–5% weight loss, positive hemoccult but no visible blood, loose/soft stools: 1; 5–10% weight loss, positive hemoccult with visual pellet bleeding, very soft stools: 2; 10–15% weight loss, blood around the rectum/prolapse, watery stools: 3.15–20% weight loss, gross bleeding, and diarrhea:4. After 12 days rats were dosed with 2 mL of encapsulated bacteria in 5 ml of PBS containing 10% wt/v sodium bicarbonate via oral gavage. Ten to 12 h following gavage, rats were separated, and fecal samples were collected, capsules were retrieved, and transferred to PBS on ice.

2.13. Stool sample preparation

Stool samples were collected from each rat prior to DSS administration and again after 12 days of DSS administration. Stools were dissolved in PBS, and a minimum of 10 capsules were retrieved from each of 3 separate stool samples from each rat. For each of the 3 stool replicates, 5 capsules were homogenized and processed as described for the bacterial biosensing assays. The remaining capsules were imaged to qualitatively assess capsule integrity following passage through the rat GI tract. From the 3 homogenized capsule samples for each rat, 1 was plated as described for the bacterial viability assays. The 3 homogenized capsule samples were processed for flow cytometry as described previously in the biosensing assays.

2.14. Intestinal sample preparation

At the time of sacrifice, the colon was separated from the cecum and rectum at the distal and proximal ends respectively. The contents of the colon were subsequently rinsed out with 10 mL of ice-cold PBS via polyurethane gavage tubing inserted into the distal end of the colon. The colon was then cut longitudinally along the mesenteric line and rinsed in a Petri dish containing ice cold PBS as described previously [47]. With the luminal side facing upwards, the colon was swiss rolled against a wooden stick beginning with the proximal end. The rolled colon was placed in a tissue cassette and stored in 10% formalin for 24 h. Then, the cassettes were transferred to 70% ethanol for at least 24 h and later processed for sectioning and H&E staining (Baylor College of Medicine Histology Core).

2.15. Transfer function modeling and parameter estimation

The transfer functions were obtained by fitting the fluorescence

values at each ligand concentration to the Hill equation, $F = A + B/(1 + (k_{1/2}/L)^n)$, using the LmFit python package for non-linear least-squares minimization and curve-fitting [48]. Here, F is the fluorescence at a given ligand concentration L, $k_{1/2}$ is the concentration of ligand that elicits a half-maximal response, n is the Hill coefficient, A is the fit of the minimum response with no ligand, and B is the fit of the maximum response at saturating ligand concentration. All transfer functions were measured for 3 independent biological replicates. Datasets from each replicate were fit independently. The 95% confidence intervals of fit parameter values were calculated using the conf_interval function in LmFit, which executes the F-test. Fit parameters for all experiments in this study are shown in Table S1. The dynamic range was measured as the ratio between the maximal and minimal response.

2.16. Statistics and data analysis

Statistical analysis was performed using the SciPy python package [49] and data was visualized using the Seaborne python package [50]. Equal sample variance was assumed for all datasets where variances were within a twofold magnitude of one another. The Shapiro-Wilk test for normality was administered to the data for each pre- and post-DSS comparison. Any comparison for a non-normal distribution was performed with the non-parametric Mann-Whitney *U* test. For *in vivo* studies, correlation was evaluated using the Pearson correlation coefficient to measure the linear relationship between bacterial fluorescence and rat DAI. The corresponding p-values were calculated assuming a normal distribution. Some data was visualized using GraphPad Prism. Flow cytometry scatter plots were visualized using FlowCal [46].

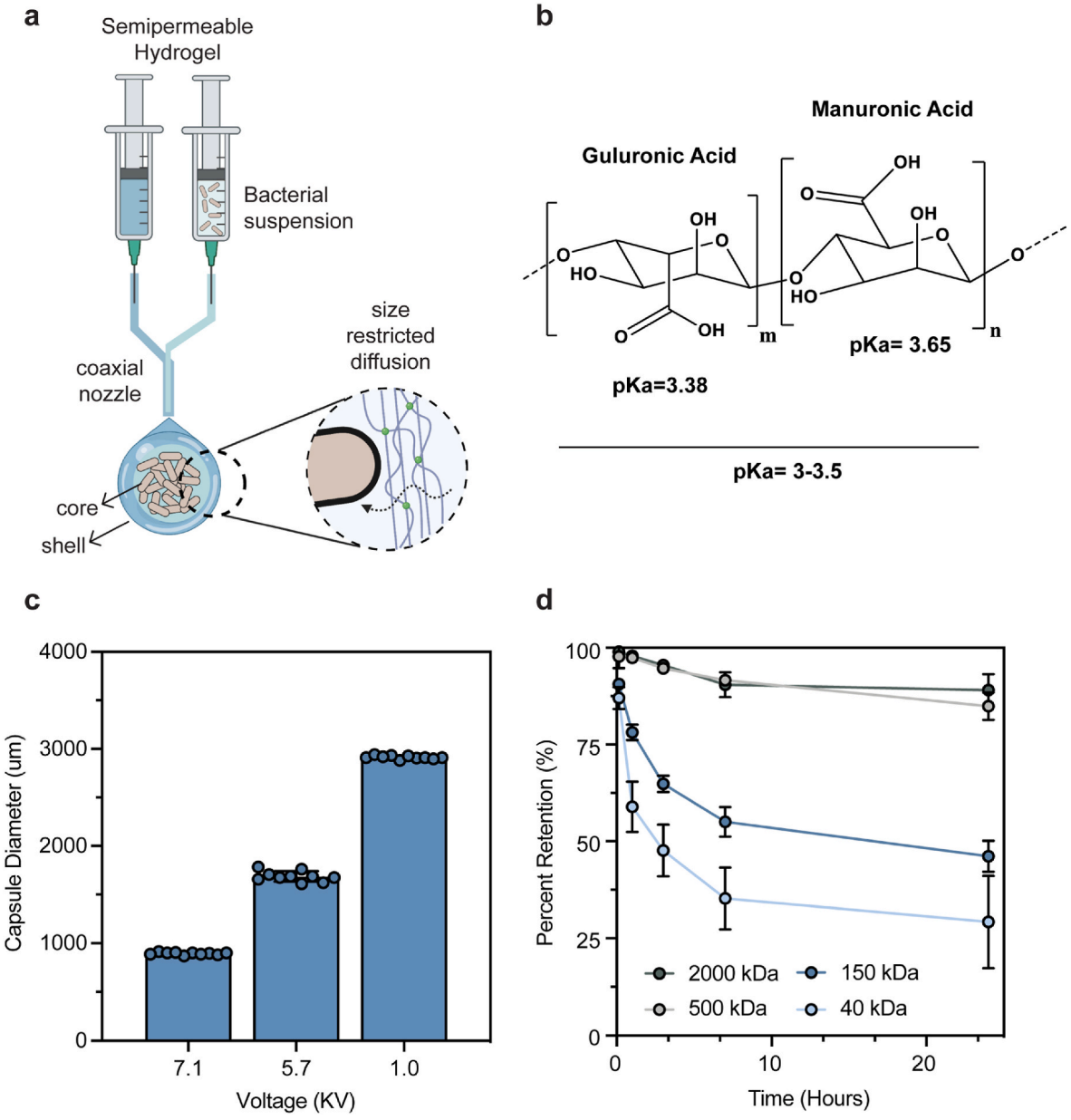

Fig. 2. Fabrication and characterization of alginate capsules. **a)** Schematic illustration of capsule synthesis. **b)** Chemical structure of alginic acid depicting associated pKa of each monomers' carboxylic acid. **c)** Capsule diameter as a factor of electrospray voltage. Each data point represents the diameter of one capsule. The blue columns and error bars represent the mean and SD, respectively, of 10 technical replicates collected on the same day. **d)** Capsule permeability to different molecular weight dextran over 24 h. Each data point represents the dextran diffusion from one capsule. The blue columns and error bars represent the mean and SD, respectively, of 5 technical replicates collected over the span of one day. (For interpretation of the references to colour in this figure legend, the reader is referred to the Web version of this article.)

Schematics were created with BioRender and Adobe Illustrator.

3. Results

3.1. Development of a bacterial encapsulation platform that preserves cell viability

For the development of our encapsulation platform, we first identified a biocompatible polymer and approach for containment of the bacteria. Specifically, we utilized a two-fluid co-axial electrostatic spraying device [51] to synthesize core-shell capsules wherein bacteria are loaded only into the core (Fig. 2a). The material selected was alginate, which when gelled has a pore size large enough to enable nutrient exchange between the encapsulated bacteria and the surrounding environment outside the capsule. Furthermore, alginate exhibits unique pH-sensitive behavior that has established the material as an acid-resistant drug carrier [52]. The polymer's chemical structure includes guluronic and mannuronic acid [53], which have pKa values of 3.38 and 3.65, respectively (Fig. 2b). Alginate increases in viscosity at low pH due to intramolecular hydrogen bonds that form after the carboxylic acid groups are protonated [54]. This pH-dependent behavior enables alginate hydrogels to protect encapsulated payloads in low pH environments, including simulated gastric fluid (SGF).

Different characteristics of the hydrogels were optimized to develop an improved system for bacterial delivery, including crosslinking bath, hydrogel size, and shell thickness. For gelation, we selected an ionic crosslinking approach due to its improved safety profile over covalent crosslinkers [55]. Specifically, barium-mediated crosslinking has been shown to form hydrogels with high structural stability. In addition, we have previously demonstrated hydrogel stability in various inflammatory conditions [56–58], thus, we chose barium chloride for the fabrication of our capsules. This encapsulation platform permits highly reproducible tuning of structural properties like hydrogel size, which can be reliably adjusted by modulating voltage (Fig. 2c). For this work, we selected capsule diameters of 1.5 mm to match the maximum gastrointestinal clearance size of rats, previously reported to be up to 2 mm [59]. A voltage of 5.7 V was found to produce 1.5 mm capsules most consistently (Standard deviation = ±54.2 μm). The shell thickness can be modified by modulating the core and shell flow rate ratios. Shell thickness is an important property that enables various degrees of separation of the encapsulated cells from the host. For this work, we used a ratio of 5:14 resulting in a core radius of 0.6 mm and a shell thickness of approximately 0.3 mm (Fig. S1). This capsule configuration results in a dense and homogenous capsule core, and further separates the engineered bacterial strain from direct contact with the host upon delivery. We assayed the permeability of our hydrogels using dextran diffusion and found that >80% of molecules greater than 500 kDa are retained over the course of 24 h (Fig. 2d). As intended, this pore size is large enough to be suitable for the size-restricted diffusion of small molecules and small enough to contain bacteria which have an approximate length of 1 μm. We hypothesized that these benefits would enable the exchange of nutrients and biomarkers between the encapsulated cells and their surrounding environment, as well as bacterial growth and physiological activity.

For microbiological analyses of encapsulated bacteria, including plating for live cell counting, and flow cytometry, encapsulated microbes need to be released from the gels. To achieve this, we developed a biocompatible method to free bacteria from the polymer matrix. We first exposed the capsules to a chelating agent, and subsequently physically homogenized the gels to disrupt the polymer. We added the metal chelator EDTA to disrupt barium crosslinks and reverse gelling, allowing for gentler mechanical disruption to be used [60]. The use of EDTA during homogenization improved the retrieval of encapsulated bacteria compared to PBS (Fig. S2a). The duration and temperature of cell retrieval was optimized such that cell viability was minimally affected and consistent among samples (Fig. S2b). The use of physical homogenization to improve hydrogel deterioration did not affect the viability of free cells (Fig. S2c).

Using the above method, we next assessed the viability of Nissle within the capsules using Syto-9 and propidium iodide cell stains. Living bacteria are stained only by SYTO-9, while non-living bacteria are stained by both SYTO-9 and propidium iodide. We confirmed proper staining of live and dead cells using heat killing of unencapsulated bacterial controls (Fig. S3a). Fluorescence microscopy of the hydrogels revealed that a majority of encapsulated bacteria remained viable, as demonstrated by the lack of red fluorescence in living cells, and CFU counts compared to heat killed controls (Fig. 3a, Fig. S3b). To quantitatively assess loss of bacteria upon encapsulation, we plated the bacteria and counted colony-forming units (CFU) of capsule volume prior to and after encapsulation (Fig. 3b). Bacterial viability prior to and following encapsulation was not significantly different ($p = 0.715$) Specifically, an average of 1.27×10^5 CFU were loaded into each capsule, and an average of 1.49×10^5 CFU were retrieved from each capsule after encapsulation.

We next explored bacterial growth within the capsules at different phases to enable identification of an optimal loading density. First, we grew Nissle cultures to an optical density at 600 nm (OD_{600}) of either 0.1 or 1 for encapsulation. Bacteria were then washed with PBS to remove media traces and concentrated 10X into a 1:19 solution of PBS:alginate, as described in Methods 2.2. The bacteria were then encapsulated as described in Methods 2.3. After encapsulation, a subset of capsules were imaged via previously established darkfield microscopy methods that enhance the contrast of the hydrogel boundary to the encapsulated bacteria [61]. Representative images of blank capsules and capsules loaded with bacteria at different optical densities, as well as blank capsules, demonstrate increased capsule core opacity as a function of loading density (Fig. 3c). We then characterized the growth of bacteria encapsulated at different phases by dissociating the gels and counting CFU at 0, 4, 8, 24, and 48 h (Fig. 3d). Bacteria encapsulated during exponential phase ($OD_{600} = 0.1$) exhibit a longer period of growth than those encapsulated closer to stationary phase ($OD_{600} = 1$). It is believed that the stability and robustness of engineered bacterial circuits is higher during exponential growth phase where continuous growth enables a steady state of biochemical reaction rates. For example, some sensors grown into stationary phase exhibit increased basal activity (leakiness) compared to exponential phase [62]. Inside the restricted microenvironment, bacteria reached an average population capacity of $2.38 \times 10^7 \pm 1.19 \times 10^7$ CFU/capsule regardless of initial growth state at the time of encapsulation. These results highlight the ability of the capsules to restrict total bacterial growth, which serves as a function of this platform in regulating bacterial delivery. Over the course of growth, the bacteria encapsulated at OD_{600} 0.1 were fixed and stained with DAPI at 0-, 8-, and 24-h following encapsulation and imaged via confocal microscopy (Fig. 3e), illustrating that the capsule microenvironment permits cell growth. To deliver engineered bacteria to the animal gut, bacteria were hereafter encapsulated at $OD_{600} = 0.1$ to best maintain near-steady state conditions and prevent loss-of-function during transport through the gastrointestinal tract (8–10 h for the rat model used in this work).

3.2. Engineered thiosulfate sensing occurs robustly in capsules

To evaluate whether encapsulation affects biosensor performance, we examined the response of a previously engineered E. *coli* strain designed to express superfolder green fluorescent protein (sfGFP) in the presence of extracellular thiosulfate [20] (Fig. 4a). This strain is also engineered to express high levels of the red fluorescent protein mCherry in a constitutive manner to facilitate differentiation from native gut bacteria. To this end we compared the transfer function, or quantitative relationship between thiosulfate concentration and sfGFP fluorescence, of non-encapsulated (free) vs. encapsulated versions of this strain. To evaluate fluorescence of encapsulated microbes, bacteria were freed from the hydrogels via EDTA chemical chelation and mechanical

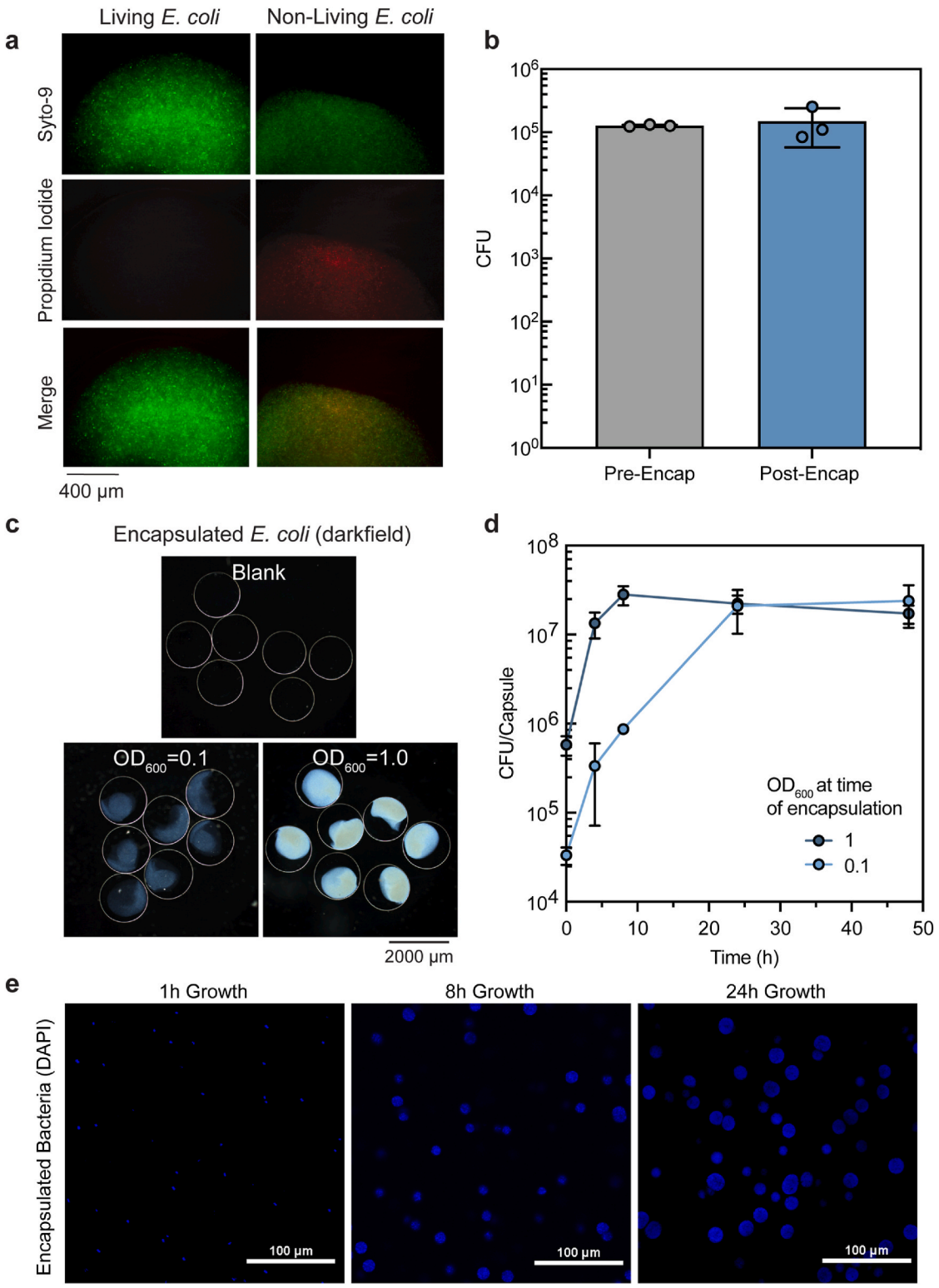

Fig. 3. Encapsulation preserves bacterial viability. a) Bacterial viability is preserved within capsules. Living bacteria accept only SYTO-9 stain while non-living bacteria accept both SYTO-9 and propidium iodide. Capsule microscopy images are representative of n = 3 biological replicates containing 5 capsules each. **b)** Bacterial viability (CFU) prior to and following encapsulation was not significantly different (p = 0.715***). Each data point represents the CFU retrieved from one capsule or one capsule core volume of free bacteria. Columns and error bars represent the mean and SD, respectively, of 3 biological replicates collected on the same day. Average bacterial load per capsule is $7.47 \times 10^4 \pm 3.74 \times 10^4$ CFU. **c)** Dark-field images of hydrogel capsules with and without encapsulated *E. coli* at varying cell densities. Images are representative of ≥60 capsules. Images were processed in photoshop for background removal. **d)** Bacteria encapsulated at OD_{600} 0.1 can grow inside capsules and reach an average carrying capacity of $2.38 \times 10^7 \pm 1.19 \times 10^7$ CFU/capsule. A similar carrying capacity is reached for bacteria encapsulated at OD_{600} 1. Data points and error bars represent the mean and SD, respectively, of 3 biological replicates collected over the course of 48 h. **e)** Bacteria encapsulated at OD_{600} 0.1 were retrieved at 3 timepoints during growth, fixed in 4% PFA, and stained with DAPI for visualization. Each blue cluster represents the stained bacteria inside one capsule. (For interpretation of the references to colour in this figure legend, the reader is referred to the Web version of this article.)

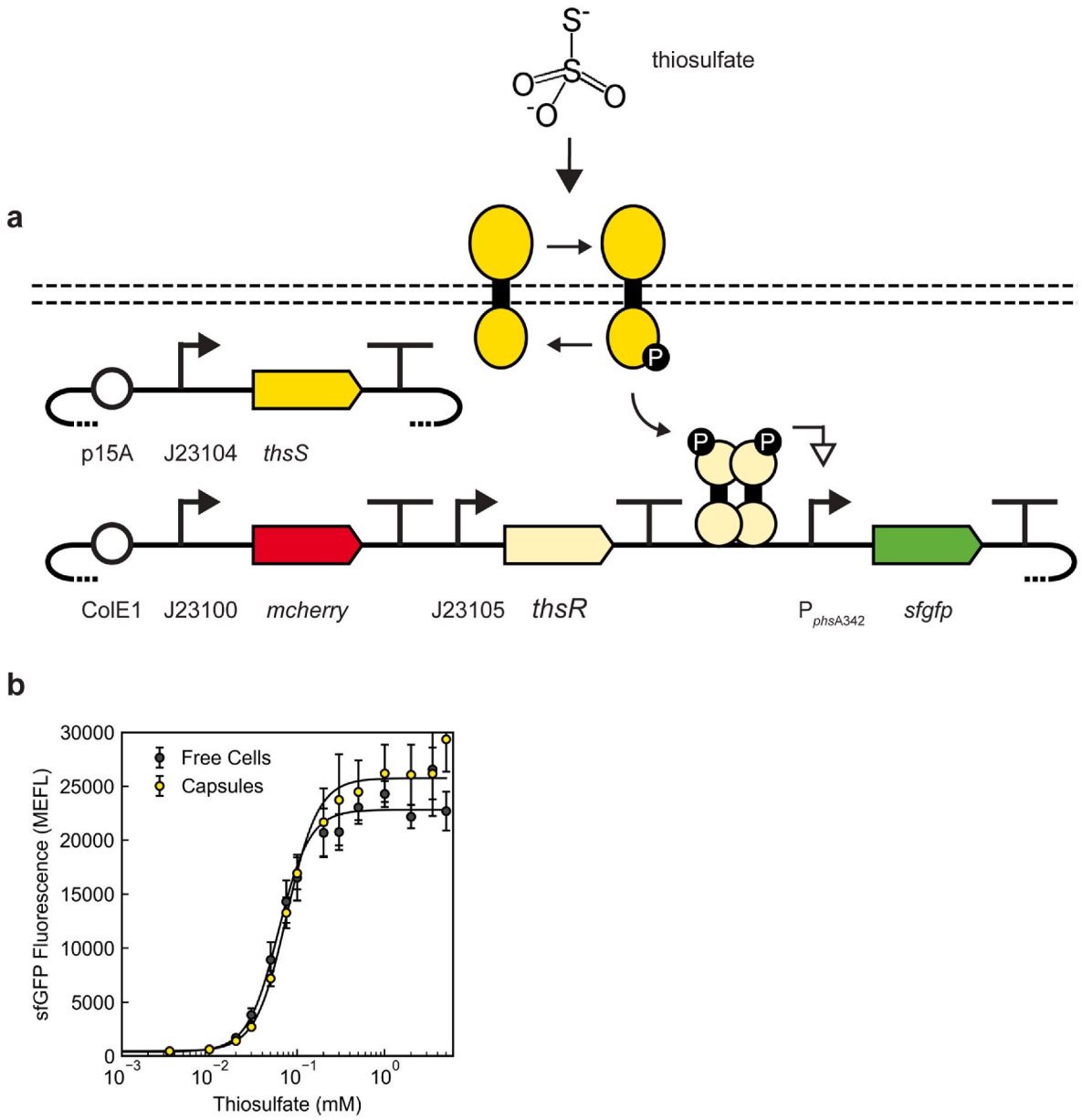

Fig. 4. Engineered *E. coli* report extracellular thiosulfate levels in capsules a) Diagram of the engineered strain used for thiosulfate sensing *in vivo*. ThsS and ThsR encode the sensor histidine kinase and response regulator comprising the thiosulfate-responsive ThsSR two-component system, respectively. P15A and ColE 1 are origins of replication of two separate plasmids used to encode the system. J23104, J23100, and J23105 are constitutive promoters used to express the system genes. $P_{phsA342}$ is the ThsR-activated promoter used to drive sfGFP expression. The constitutive mCherry fluorescent protein is included to enable rapid identification from native stool microbiota. **b)** Thiosulfate dose-response is preserved following encapsulation of ThsSR sensor bacteria. Data points and error bars represent the mean and SD, respectively, of 3 biological replicates collected on the same day. Fit lines are Hill functions as described in Methods 2.14, and fit parameters are given in Table S1. Dynamic range, $K_{1/2}$, and hill coefficient are similar prior to and following encapsulation.

disruption via electric homogenizer as described above. They were then processed as described in Methods 2.8–2.9 for analysis via flow cytometry (Fig. S4). We found strong quantitative correspondence between the thiosulfate responses of the free and encapsulated cells, and no statistical significance between the response of each group indicating that sensor function is preserved after encapsulation (Fig. 4b, Table S1). Furthermore, constitutive mCherry expression was unaffected by both thiosulfate concentration and encapsulation (Fig. S5). Finally, we confirmed that the addition of 5% DSS to the bacterial growth media did not impact the thiosulfate response in capsules (Fig. S6). Based on these results, we determined that our encapsulated thiosulfate-sensing *E. coli* can likely be used to evaluate DSS-induced colitis *in vivo*.

3.3. Encapsulated bacteria robustly survive passage through the rodent gastrointestinal tract

The gastrointestinal environment has extremities that may reduce bacterial viability *in vivo*. To predict the survival of our encapsulated bacteria upon oral administration, we examined the ability of our capsules to protect bacteria at the acidic pH levels of the stomach *in vitro*. In particular, we incubated encapsulated bacteria in media buffered to pH = 3.2 with hydrochloric acid (HCl), which is the acidic component of gastrointestinal (GI) fluid [63]. We incubated approximately 1.6×10^5 CFU of free and encapsulated bacteria at 37 °C in the acidified media for 2 and 6 h and measured their viability via CFU. Free bacteria demonstrated significantly lower viability at both 2 h (0.04%), and 6 h (0%)

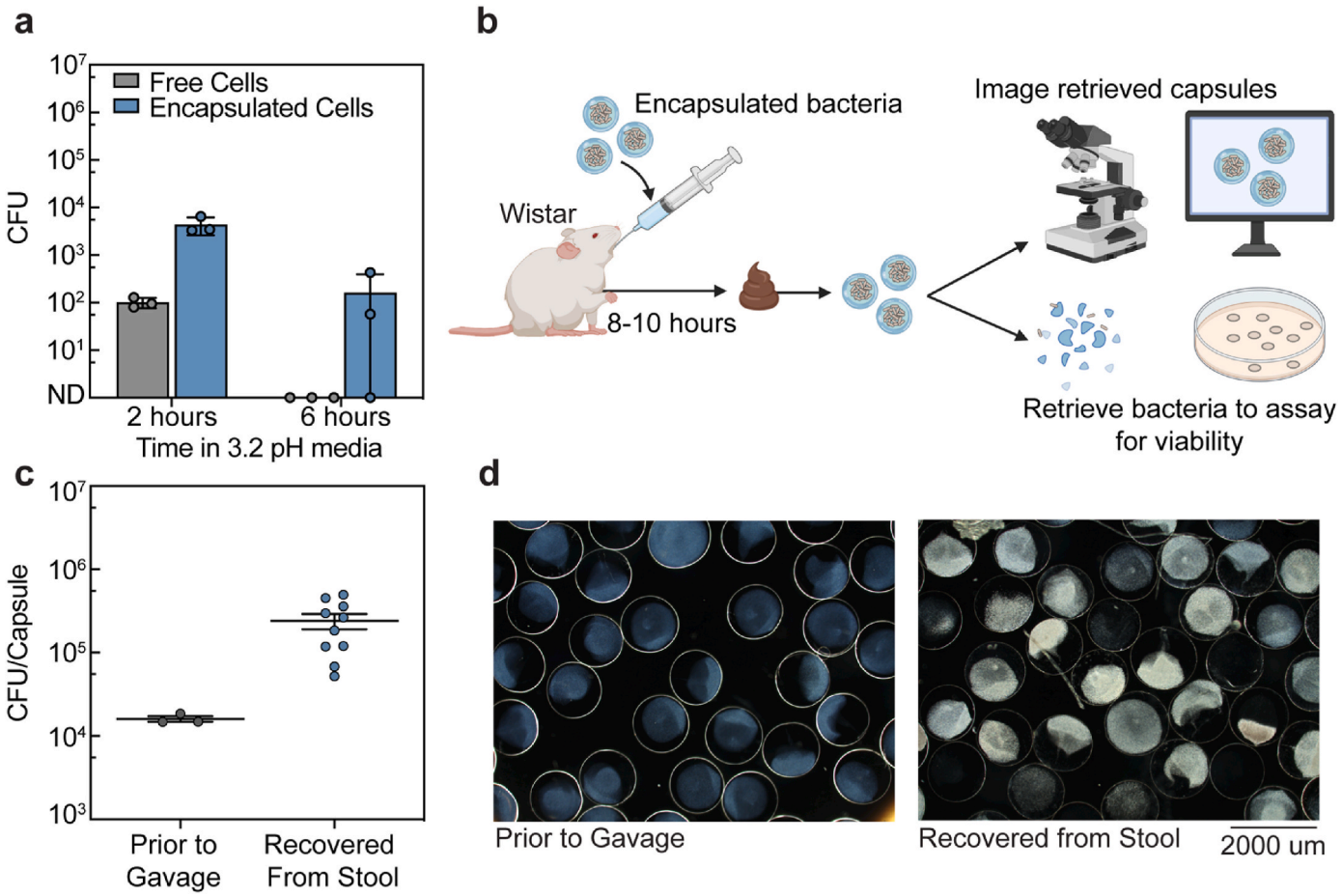

Fig. 5. Encapsulation preserves bacterial viability in the rat GI tract. a) Encapsulated bacteria survive in acidic conditions. Each data point represents the CFU retrieved from one capsule or one capsule core volume of free bacteria. Columns and error bars represent the mean and SD, respectively, of 3 biological replicates collected on the same day. **b)** Schematic illustration of capsule delivery, retrieval, and post-collection processing. **c)** Bacterial viability (CFU) within capsules prior to oral administration (n = 3, mean ± SEM) and following retrieval from stool samples (n = 10, mean ± SEM) **d)** Representative darkfield images of encapsulated bacteria prior to gavage and following retrieval from stool samples. Images are representative of all capsules retrieved (between 1 and 2 mL capsule volume).

(Fig. 5a). Meanwhile, encapsulated bacteria had a 46-fold higher percent of viable bacteria at each time point (1.84% and 0.07% at 2 and 6 h respectively) compared to free bacteria. Darkfield microscopy of the gels revealed that this acidic pH treatment has minimal impact on capsule integrity (Fig. S7a). These results suggest that encapsulation may increase the viability of engineered bacteria passing through the stomach.

To examine whether these results were sustained *in vivo*, we delivered equal amounts of free or encapsulated biosensor bacteria to healthy rats (Fig. 5b). Encapsulation protected bacteria against low pH *in vitro*, but the *in vivo* stomach and intestinal environments introduce additional challenges to survival that cannot be completely modeled *in vitro*. To help address these challenges, we evaluated delivery of bacteria in PBS as well as sodium bicarbonate gavage buffer, which has been used previously to improve the viability of living cells delivered to the animal gut [64].

First, we investigated the transit time through the rat GI tract (Fig. S8a&b). We found that bacterial recovery from the stool was highest and most consistent for both capsules and free bacteria at 10 h following administration irrespective of gavage buffer. On average, out of the approximately 840 capsules delivered, 43 were recovered for PBS, and 81 were recovered for sodium bicarbonate at this time point. All subsequent experiments were therefore performed by retrieving stool samples at this timepoint. We then compared the recovery of viable bacteria from the rat stool, as measured by CFU per milligram of stool (Fig. S9a). Compared to free cells delivered in the same gavage buffer, we evaluated a 65-fold higher bacterial recovery from rats gavaged with capsules in sodium bicarbonate buffer, and 51-fold higher for those gavaged in only PBS. This suggests that while encapsulation alone can improve bacterial recovery, delivery in sodium bicarbonate can be used to further improve viability. Retrieval of diagnostic bacteria was also enhanced when using encapsulation due to the visibility of the spheres after PBS dissolution (Fig. S9b). In addition, the bacterial extraction protocol for capsules is more rapid than that for free bacteria directly from stool (Methods 2.9). Irrespective of gavage buffer, capsule morphology remained structurally similar after passage through the animal gut, suggesting that the harsh GI environments are tolerated by alginate hydrogels (Fig. S10a).

Finally, we compared the average bacterial population within capsules prior to and following passage through the rat gut (Fig. 5c). Capsules retrieved from the stool contained more bacteria on average when gavaged with sodium bicarbonate, indicating that encapsulated bacteria not only survive but grow during passage through the GI tract. This phenomenon was not observed when capsules were delivered in PBS or saline (Fig. S10b). The increased bacterial density of capsules gavaged with sodium bicarbonate is visible via darkfield microscopy (Fig. 5d). Capsule cores recovered from stool are visibly more opaque than those imaged prior to gavage. This increase in viability and sample retention enabled the administration of significantly fewer (100x) bacteria per gram body weight than described in previous studies (approximately 10^9 CFU/g in mice vs. 10^7 CFU/g in rats for this study) and demonstrated increased efficiency in diagnostic capabilities through the use of

our platform [20].

3.4. Encapsulated bacteria diagnose DSS-induced colitis

Healthy animals should have minimal levels of local thiosulfate and thus, encapsulated cells should have only basal expression of the sfGFP reporter. To evaluate whether any changes in sfGFP expression occur in healthy animals, prior to disease development, encapsulated bacteria administered in sodium bicarbonate were evaluated for fluorescent expression (Fig. 6a). Specifically, 2 mL of encapsulated ThsSR were orally gavaged to rats (n = 10). The following day, capsules were retrieved from fresh fecal pellets and processed for flow cytometry as described previously. Flow analysis demonstrated that mean fluorescence intensity of encapsulated ThsSR retrieved from healthy animals did not have a significant increase in sfGFP expression compared to baseline, confirming that the sensor strain is sensitive to its biomarker *in vivo* (Fig. 6b).

The dextran sulfate sodium (DSS)-induced colitis model is a widely accepted model for establishment of inflammatory bowel disease. To determine the success of our encapsulated biosensor platform in diagnosing the extent of disease progression in this model, we treated rats (n = 10) with DSS in their drinking water for 12 days (Fig. 6a). Throughout

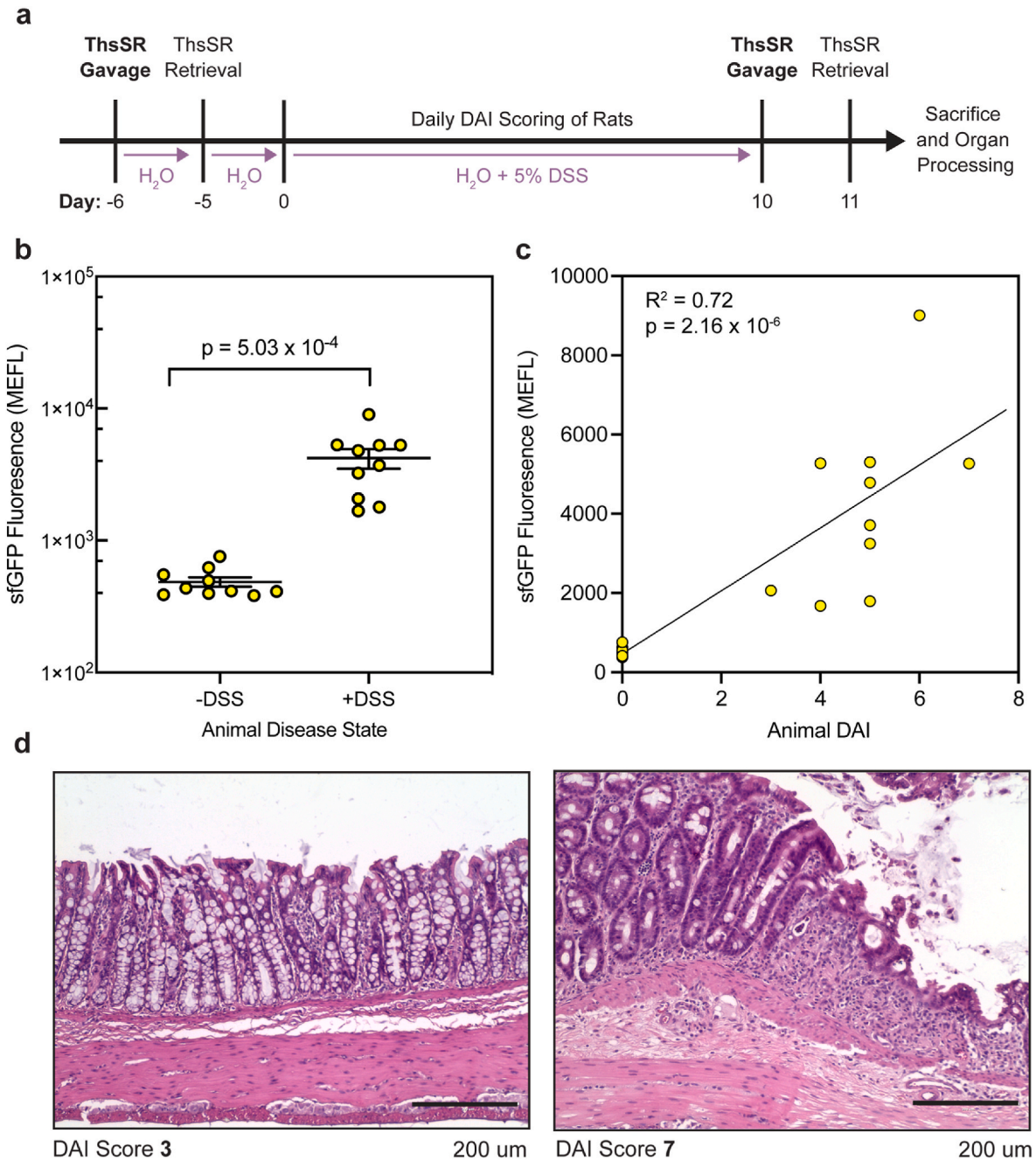

Fig. 6. Encapsulated bacteria diagnose colitis in a rat DSS model. a) Timeline of disease development, capsule dosing, and sample processing. **b)** sfGFP expression of encapsulated ThsSR sensor bacteria retrieved from fecal samples prior to and after treatment with DSS. Each data point represents the mean fluorescence of 3 technical replicates collected from each rat. Each technical replicate represents the geometric mean fluorescence of cells collected from 5 capsules (mean ± SEM). **c)** sfGFP expression of encapsulated ThsSR sensor bacteria correlates positively with animal DAI. Each data point represents the mean fluorescence of 3 technical replicates collected from each rat. **d)** Representative histological sections from rats with varying degrees of inflammation and different DAI. 5 images were acquired per rat. Rats were sacrificed at day 11 and colon sections were processed. At this point, rats had reached different final DAI states.

this time, the disease activity index (DAI) of each rat was reported based on changes in body weight (Fig. S11a), presence of occult blood in the stool, and stool consistency. The index is used to assess the degree of GI disruption. Here, we saw variable increases in DAI score across animals in response to DSS treatment, with the average DAI score across animals reaching 5.5±1.3 by day 12 (Fig. S11b). After 12 days of DSS treatment, encapsulated thiosulfate sensing bacteria were delivered to each rat via oral gavage. The following day, gels were retrieved from the stool and processed. Spleens from each animal were also collected and weighed (Fig. S11c).

Following capsule retrieval, we analyzed our engineered bacteria by flow cytometry. Cells were gated by an FSC/SSC scatter profile characteristic of Nissle, discarding counts with an mCherry fluorescence value lower than 5000 MECY, in order to isolate only the engineered ThsSR Nissle for analysis. Bacterial samples with fewer than 250 cells following gating by these criteria were discarded (Fig. S12a). Overall, our high sample retention suggests that encapsulation could improve the confidence of diagnosis compared to the use of free cells, by producing more tractable samples.

Consistent with our prior results with free bacteria, we observed strong ThsSR activation following DSS treatment as compared to pre-DSS, demonstrated by significant increases in sfGFP expression (Fig. 6b). We found that sfGFP fluorescence levels correlate linearly with DAI at the time of capsule administration (Fig. 6c), suggesting the ability of our platform to be used as a means of measuring disease onset and progression. In addition to DAI, disease extent was characterized via histological sectioning and H&E staining of GI tissue (Fig. S13). At the study endpoint, the colon of each rat was excised and sectioned, and imaged. Representative images of intestinal sections from rats with low (3) and high (7) DAI scores are shown, depicting a relationship between DAI score and visible degree of epithelial damage (Fig. 6d). Together these results demonstrate that ThsSR activation *in vivo* correlated with disease progression as measured by multiple metrics, including a visual assessment of physical tissue damage.

4. Discussion

In this study, a platform was established to improve the delivery and retrieval of engineered metabolite-sensing bacteria to and from the animal gastrointestinal tract. Specifically, genetically engineered bacterial biosensors were encapsulated in a hydrogel matrix and deployed in an animal model of gut inflammation where they sensed and responded to an internal disease state. This technology has the potential to address current drawbacks in diagnosis of gastrointestinal inflammation and may significantly improve quality of life for affected patients.

Since the approval of natural probiotics in the food industry, researchers have focused on the use of these bacteria for various biomedical applications such as cancer, diabetes, and IBD [65–67]. Oral delivery is the most convenient and widely used method for the administration of natural and engineered probiotics to patients. However, the low pH in the gastrointestinal environment can negatively affect bacterial viability. Therefore, encapsulation of bacteria within a protective matrix could improve bacterial viability *in vivo*. Recently, polymer-based encapsulation has been applied to many engineered microbial biosensors including a heavy-metal sensing strain [68], an L-lactate biosensing strain [69], and an autoinducer responsive strain [65] for improved containment and viability in harsh environmental or *in vitro* applications. However, this technique can be similarly applied to biosensors engineered for detection of disease biomarkers *in vivo*. Several such biosensors have been developed including a nitric oxide sensing strain [66], as well as thiosulfate and tetrathionate sensors developed previously by our group and others [20,67]. However, to our knowledge, no previous research has directly measured the survival of encapsulated biosensor bacteria upon retrieval in a mammalian model. The majority of therapeutic and diagnostic bacterial systems developed to date have been tested primarily in *in vitro* digestion models that are unable to accurately simulate the animal GI tract [37]. Here, macroscale alginate capsules were generated to both improve viability of orally delivered biosensor bacteria, and to localize bacteria into concentrated particles, thereby improving sample recovery from stool and providing a more suitable alternative for the delivery of diagnostic bacteria.

Diagnostic tools are essential in the care of patients with inflammatory diseases such as IBD. In this disease, patients who experience delays between symptom onset and diagnosis are at increased risk of emergency surgery and more likely to require colectomy [70–77]. Thus, the development of reliable, non-invasive diagnostic tools could result in a significant improvement in disease management and quality of life for patients suffering from IBD and other chronic illnesses [78]. Importantly, this platform can be readily translated to the clinic. Both the hydrogel formulation, and the bacterial chassis are currently approved for human use in several countries (NCT05538624, NCT04541628, NCT04787276, NCT02276508). Furthermore, given the flexibility of bacterial engineering, future iterations of this platform could explore multiplexing for generation of more informed diagnostics capable of detecting multiple biomarkers. This would provide comprehensive insight into the gut microenvironment and individual disease state. Moreover, delivery of a closed loop system whereby biomarker recognition initiates the production of therapeutic proteins is enabled by this platform. Such a design would present an alternative to the current standard of care which involves an intensive regimen of intravenously administered corticosteroids [79] (NCT05587673), or chronic immunosuppression [80–83].

In conclusion, our platform will support progress towards the improved administration, safety, and retrieval of engineered probiotic bacteria for diagnostic applications. Additionally, the innovations presented herein will improve the generalizability and application of synthetic biology approaches for human health. Living microbial diagnostics that can detect inflammation *in situ* could overcome many challenges associated with the current standard of care for IBD. In addition to IBD, the mammalian colon is an important target for many other localized and systemic conditions. The human metabolism, immune, and brain function are all affected by gut processes, which are orchestrated in part by metabolic and signaling interactions among host cells and the resident microbiota [7, 84–86]. Overall, dysbiosis in the gut microbiome is tied to many aspects of human health, and encapsulation of genetically engineered sensor bacteria has untapped potential as a tool to analyze, target, and treat this dynamic and inaccessible microenvironment.

Author contribution statement

Jeffrey J. Tabor: Conceptualization, verification, resources, writing-review and editing, supervision, project administration, funding acquisition **Omid Veiseh**: Conceptualization, verification, resources, writing-review and editing, supervision, project administration, funding acquisition **Samira Aghlara-Fotovat:** Conceptualization, methodology, validation, formal analysis, investigation, data curation, writing-original draft, writing-review and editing, visualization, project administration **Elena Musteata**: Conceptualization, methodology, validation, formal analysis, investigation, data curation, writing-original draft, writing-review and editing, visualization, project administration **Moshe Baruch**: Conceptualization and investigation **Michael D. Doerfert**: Investigation **Maya Levitan**: Investigation.

Declaration of competing interest

The authors declare the following financial interests/personal relationships which may be considered as potential competing interests: Omid Veiseh and Jeffrey Tabor reports a relationship with Pana Bio that includes: board membership and equity or stocks. Samira Aghlara-Fotovat, Elena Musteata, Michael D. Doerfert, Moshe Baruch, Jeffrey J. Tabor, Omid Veiseh has patent pending to Pana Bio. Moshe Baruch is

current employee of Pana Bio.

Data availability

Data will be made available on request.

Acknowledgements

We thank Ryan Butcher for performing microscopy analysis for the free cell viability assays and Sudip Mukherjee for guidance with chemical characterization. We thank Dr. Joel Moake and his lab for sharing their flow cytometer. This work was supported by NSF CAREER 1553317 and NIH R01AI155586 (Tabor), National Institute of Health grant 1RO1DK120459-01 (Veiseh), and a Rice University seed grant (Tabor and Veiseh). E.M. was supported by a National Science Foundation (NSF) Graduate Research Fellowship under Grant No. 1842494.

Appendix A. Supplementary data

Supplementary data to this article can be found online at https://doi.org/10.1016/j.biomaterials.2023.122246.

References

[1] R. Sender, S. Fuchs, R. Milo, Are we really vastly outnumbered? Revisiting the ratio of bacterial to host cells in humans, Cell 164 (2016) 337–340.
[2] R.E. Ley, D.A. Peterson, J.I. Gordon, Ecological and evolutionary forces shaping microbial diversity in the human intestine, Cell 124 (2006) 837–848.
[3] K. Dabke, G. Hendrick, S. Devkota, The gut microbiome and metabolic syndrome, J. Clin. Invest. 129 (2019) 4050–4057.
[4] J.-S. Hwang, C.-R. Im, S.-H. Im, Immune disorders and its correlation with gut microbiome, Immune Netw 12 (2012) 129–138.
[5] J.F. Cryan, K.J. O'Riordan, K. Sandhu, V. Peterson, T.G. Dinan, The gut microbiome in neurological disorders, Lancet Neurol. 19 (2020) 179–194.
[6] J. Halfvarson, et al., Dynamics of the human gut microbiome in inflammatory bowel disease, 2017, Nat. Microbiol. 25 (2) (2017) 1–7.
[7] B. Han, et al., Microbial genetic composition tunes host longevity, Cell 169 (2017) 1249–1262.e13.
[8] A.B. Shreiner, J.Y. Kao, V.B. Young, The gut microbiome in health and in disease, Curr. Opin. Gastroenterol. 31 (2015) 69.
[9] W.M. de Vos, H. Tilg, M. Van Hul, P.D. Cani, Gut microbiome and health: mechanistic insights, Gut 71 (2022) 1020.
[10] M.G. Rooks, W.S. Garrett, Gut microbiota, metabolites and host immunity, 2016, Nat. Rev. Immunol. 166 16 (2016) 341–352.
[11] A. Agus, K. Clément, H. Sokol, Gut microbiota-derived metabolites as central regulators in metabolic disorders, Gut 70 (2021) 1174–1182.
[12] A. Metwaly, S. Reitmeier, D. Haller, Microbiome risk profiles as biomarkers for inflammatory and metabolic disorders, 2022, Nat. Rev. Gastroenterol. Hepatol. 196 (19) (2022) 383–397.
[13] E.S. Zhgun, E.N. Ilyina, Fecal metabolites as non-invasive biomarkers of gut diseases, Acta Naturae 12 (2020) 4.
[14] B.P. Landry, J.J. Tabor, Engineering diagnostic and therapeutic gut bacteria, Microbiol. Spectr. 5 (2017) 1–22.
[15] D.T. Riglar, P.A. Silver, Engineering bacteria for diagnostic and therapeutic applications, 2018, Nat. Rev. Microbiol. 164 (16) (2018) 214–225.
[16] M. Hicks, T.T. Bachmann, B. Wang, Synthetic biology enables programmable cell-based biosensors, ChemPhysChem 21 (2020) 132–144.
[17] M.R. Charbonneau, V.M. Isabella, N. Li, C.B. Kurtz, Developing a new class of engineered live bacterial therapeutics to treat human diseases, 2020, Nat. Commun. 111 (11) (2020) 1–11.
[18] A. Cubillos-Ruiz, et al., Engineering living therapeutics with synthetic biology, Nat. Rev. Drug Discov. (2021), 0123456789.
[19] M.P. McNerney, K.E. Doiron, T.L. Ng, T.Z. Chang, P.A. Silver, Theranostic cells: emerging clinical applications of synthetic biology, Nat. Rev. Genet. 22 (2021) 730–746.
[20] K.N. Daeffler, et al., Engineering bacterial thiosulfate and tetrathionate sensors for detecting gut inflammation, Mol. Syst. Biol. 13 (2017) 923.
[21] I.M. Cartwright, et al., Mucosal acidosis elicits a unique molecular signature in epithelia and intestinal tissue mediated by GPR31-induced CREB phosphorylation, Proc. Natl. Acad. Sci. U.S.A. 118 (2021).
[22] J.M. Pickard, et al., Rapid fucosylation of intestinal epithelium sustains host–commensal symbiosis in sickness, 514, 2014, pp. 638–641. Nat. 2014 5147524.
[23] M. Mimee, A.C. Tucker, C.A. Voigt, T.K. Lu, Programming a human commensal bacterium, Bacteroides thetaiotaomicron, to sense and respond to stimuli in the murine gut microbiota, Cell Syst 1 (2015) 62–71.
[24] D.T. Riglar, et al., Engineered bacteria can function in the mammalian gut long-term as live diagnostics of inflammation, Nat. Biotechnol. 35 (2017) 653–658.
[25] S. Han, et al., Probiotic gastrointestinal transit and colonization after oral administration: a long journey, Front. Cell. Infect. Microbiol. 11 (2021) 102.
[26] M.R. Charbonneau, V.M. Isabella, N. Li, C.B. Kurtz, Developing a new class of engineered live bacterial therapeutics to treat human diseases, Nat. Commun. 11 (2020) 1–11.
[27] Z. Jiang, M. Li, D.J. McClements, X. Liu, F. Liu, Recent advances in the design and fabrication of probiotic delivery systems to target intestinal inflammation, Food Hydrocolloids 125 (2022), 107438.
[28] S. Fujimori, Gastric acid level of humans must decrease in the future, World J. Gastroenterol. 26 (2020) 6706.
[29] L. Cassani, A. Gomez-Zavaglia, J. Simal-Gandara, Technological strategies ensuring the safe arrival of beneficial microorganisms to the gut: from food processing and storage to their passage through the gastrointestinal tract, Food Res. Int. 129 (2020), 108852.
[30] K. Feng, et al., A novel route for double-layered encapsulation of probiotics with improved viability under adverse conditions, Food Chem. 310 (2020), 125977.
[31] C.M. Cremers, D. Knoefler, V. Vitvitsky, R. Banerjee, U. Jakob, Bile salts act as effective protein-unfolding agents and instigators of disulfide stress in vivo, Proc. Natl. Acad. Sci. U.S.A. 111 (2014) E1610.
[32] X. Liu, M.E. Inda, Y. Lai, T.K. Lu, X. Zhao, Engineered living hydrogels, Adv. Mater. 34 (2022), 2201326.
[33] D.K. Nguyen, Y.M. Son, N.E. Lee, Hydrogel encapsulation of cells in core-shell microcapsules for cell delivery, Adv. Healthc. Mater. 4 (2015) 1537–1544.
[34] K. Sultana, et al., Encapsulation of probiotic bacteria with alginate-starch and evaluation of survival in simulated gastrointestinal conditions and in yoghurt, Int. J. Food Microbiol. 62 (2000) 47–55.
[35] T.Y. Sheu, R.T. Marshall, Microentrapment of lactobacilli in calcium alginate gels, J. Food Sci. 58 (1993) 557–561.
[36] L. Angélica Andrade Lopes, et al., Microencapsulation of Lactobacillus acidophilus La-05 and incorporation in vegan milks: physicochemical characteristics and survival during storage, exposure to stress conditions, and simulated gastrointestinal digestion, Food Res. Int. 135 (2020), 109295.
[37] X. Wang, et al., Microencapsulating alginate-based polymers for probiotics delivery systems and their application, Pharmaceuticals 15 (2022).
[38] S. Prakash, T.M.S. Chang, Microencapsulated genetically engineered live E. coli DH5 cells administered orally to maintain normal plasma urea level in uremic rats, Nat. Med. 2 (1996) 883–887.
[39] D.W. Zheng, et al., An orally delivered microbial cocktail for the removal of nitrogenous metabolic waste in animal models of kidney failure, Nat. Biomed. Eng. 4 (2020) 853–862.
[40] M. Yao, et al., Improved functionality of Ligilactobacillus salivarius Li01 in alleviating colonic inflammation by layer-by-layer microencapsulation, 2021, npj Biofilms Microbiomes 71 (7) (2021) 1–10.
[41] C. Yang, et al., Upconversion optogenetic micro-nanosystem optically controls the secretion of light-responsive bacteria for systemic immunity regulation, Commun. Biol. 3 (2020) 1–14.
[42] Z. Dai, et al., Versatile biomanufacturing through stimulus-responsive cell–material feedback, Nat. Chem. Biol. 15 (2019) 1017–1024.
[43] C. Han, et al., Hydrogel microcapsules containing engineered bacteria for sustained production and release of protein drugs, Biomaterials 287 (2022), 121619.
[44] E.L. McConnell, A.W. Basit, S. Murdan, Measurements of rat and mouse gastrointestinal pH, fluid and lymphoid tissue, and implications for in-vivo experiments, J. Pharm. Pharmacol. 60 (2010) 63–70.
[45] S. Mukherjee, et al., Screening hydrogels for antifibrotic properties by implanting cellularly barcoded alginates in mice and a non-human primate, Nat. Biomed. Eng. 2023 (2023) 1–20, https://doi.org/10.1038/s41551-023-01016-2.
[46] S.M. Castillo-Hair, et al., FlowCal: a user-friendly, open source software tool for automatically converting flow cytometry data from arbitrary to calibrated units, ACS Synth. Biol. 5 (2016) 774–780.
[47] A.B. Bialkowska, A.M. Ghaleb, M.O. Nandan, V.W. Yang, Improved Swiss-rolling technique for intestinal tissue preparation for immunohistochemical and immunofluorescent analyses, J. Vis. Exp. 2016 (2016).
[48] M. Newville, et al., Lmfit: Non-Linear Least-Square Minimization and Curve-Fitting for Python, Astrophysics Source Code Library, 2016, ascl:1606.014.
[49] P. Virtanen, et al., SciPy 1.0: fundamental algorithms for scientific computing in Python, 2020, Nat. Methods 173 (17) (2020) 261–272, https://ui.adsabs.harvard.edu/abs/2016ascl.soft06014N/abstract.
[50] M.L. Waskom, seaborn: statistical data visualization, J. Open Source Softw. 6 (2021) 3021.
[51] R.K. Ghanta, et al., Immune-modulatory alginate protects mesenchymal stem cells for sustained delivery of reparative factors to ischemic myocardium, Biomater. Sci. 8 (2020) 5061–5070.
[52] M. Mansourpour, et al., Development of acid-resistant alginate/trimethyl chitosan nanoparticles containing cationic β-cyclodextrin polymers for insulin oral delivery, 2015, AAPS PharmSciTech 164 (16) (2015) 952–962.
[53] J.J. Chuang, et al., Effects of pH on the shape of alginate particles and its release behavior, Int. J. Polym. Sci. 2017 (2017).
[54] M. Rizwan, et al., pH sensitive hydrogels in drug delivery: brief history, properties, swelling, and release mechanism, material selection and applications, 2017, Polym 9 (137 9) (2017) 137.
[55] A.N. Jătariu, M. Popa, S. Curteanu, C.A. Peptu, Covalent and ionic co-cross-linking–an original way to prepare chitosan-gelatin hydrogels for biomedical applications, J. Biomed. Mater. Res. 98 (2011) 342–350.
[56] Ý.A. Mørch, I. Donati, B.L. Strand, G. Skjåk-Bræk, Effect of Ca2+, Ba2+, and Sr2+ on alginate microbeads, Biomacromolecules 7 (2006) 1471–1480.

[57] A.M. Nash, et al., Clinically translatable cytokine delivery platform for eradication of intraperitoneal tumors, Sci. Adv. 8 (2022).
[58] A.M. Nash, et al., Activation of adaptive and innate immune cells via localized Interleukin-2 cytokine factories eradicates mesothelioma tumors, Clin. Cancer Res. OF1–OF15 (2022), https://doi.org/10.1158/1078-0432.CCR-22-1493.
[59] S.F. Jang, et al., Size discrimination in rat and mouse gastric emptying, Biopharm. Drug Dispos. 34 (2013) 107–124.
[60] B.H. Chueh, et al., Patterning alginate hydrogels using light-directed release of caged calcium in a microfluidic device, Biomed. Microdevices 121 (12) (2009) 145–151, 2009.
[61] A.J. Vegas, et al., Combinatorial hydrogel library enables identification of materials that mitigate the foreign body response in primates, Nat. Biotechnol. 34 (2016) 345–352.
[62] A.J. Meyer, T.H. Segall-Shapiro, E. Glassey, J. Zhang, C.A. Voigt, Escherichia coli "Marionette" strains with 12 highly optimized small-molecule sensors, Nat. Chem. Biol. 15 (2019) 196–204.
[63] T.C. Martinsen, R. Fossmark, H.L. Waldum, The phylogeny and biological function of gastric juice—microbiological consequences of removing gastric acid, Int. J. Mol. Sci. 20 (2019).
[64] B.B. Hsu, et al., In situ reprogramming of gut bacteria by oral delivery, Nat. Commun. 11 (2020) 5030.
[65] P. Li, M. Müller, M.W. Chang, M. Frettlöh, H. Schönherr, Encapsulation of autoinducer sensing reporter bacteria in reinforced alginate-based microbeads, ACS Appl. Mater. Interfaces 9 (2017) 22321–22331.
[66] E.J. Archer, A.B. Robinson, G.M. Süel, Engineered E. coli that detect and respond to gut inflammation through nitric oxide sensing, ACS Synth. Biol. 1 (2012) 451–457.
[67] D.T. Riglar, et al., Engineered bacteria can function in the mammalian gut long-term as live diagnostics of inflammation, Nat. Biotechnol. 35 (2017) 653–658.
[68] T.C. Tang, et al., Hydrogel-based biocontainment of bacteria for continuous sensing and computation, Nat. Chem. Biol. 17 (2021) 724–731.
[69] I. Moya-Ramírez, et al., Polymer encapsulation of bacterial biosensors enables coculture with mammalian cells, ACS Synth. Biol. 11 (2022) 1303–1312.
[70] Z. Hong, et al., Delayed diagnosis is associated with early and emergency need for first Crohn's disease-related intestinal surgery, Med. Sci. Monit. 23 (2017) 4841.
[71] D.W. Lee, et al., Diagnostic delay in inflammatory bowel disease increases the risk of intestinal surgery, World J. Gastroenterol. 23 (2017) 6474.
[72] E. Safroneeva, et al., Impact of the early use of immunomodulators or TNF antagonists on bowel damage and surgery in Crohn's disease, Aliment. Pharmacol. Ther. 42 (2015) 977–989.
[73] V. Chhaya, et al., Impact of early thiopurines on surgery in 2770 children and young people diagnosed with inflammatory bowel disease: a national population-based study, Aliment. Pharmacol. Ther. 42 (2015) 990–999.
[74] F. Magro, et al., Is it possible to change phenotype progression in Crohn's disease in the era of immunomodulators? Predictive factors of phenotype progression, Am. J. Gastroenterol. 109 (2014) 1026–1036.
[75] M. Aloi, et al., Effect of early versus late azathioprine therapy in pediatric ulcerative colitis, Inflamm. Bowel Dis. 22 (2016) 1647–1654.
[76] C.S.J. Probert, A.U. Dignass, S. Lindgren, M. Oudkerk Pool, P. Marteau, Combined oral and rectal mesalazine for the treatment of mild-to-moderately active ulcerative colitis: rapid symptom resolution and improvements in quality of life, J. Crohns. Colitis 8 (2014) 200–207.
[77] D.R. Berg, J.F. Colombel, R. Ungaro, The role of early biologic therapy in inflammatory bowel disease, Inflamm. Bowel Dis. 25 (2019) 1896–1905.
[78] J. Blackwell, et al., Prevalence and duration of gastrointestinal symptoms before diagnosis of inflammatory bowel disease and predictors of timely specialist review: a population-based study, J. Crohn's and Colitis 15 (2021).
[79] S.C. Truelove, D.P. Jewell, Intensive intravenous regimen for severe attacks of ulcerative colitis, Lancet (London, England) 1 (1974) 1067–1070.
[80] K. Papamichael, et al., Infliximab in inflammatory bowel disease, Ther. Adv. Chronic Dis. 10 (2019).
[81] J.F. Colombel, et al., Infliximab, azathioprine, or combination therapy for Crohn's disease, N. Engl. J. Med. 362 (2010) 1383–1395.
[82] R. Khanna, et al., Early combined immunosuppression for the management of Crohn's disease (REACT): a cluster randomised controlled trial, Lancet (London, England) 386 (2015) 1825–1834.
[83] K. Papamichael, et al., Proactive infliximab optimisation using a pharmacokinetic dashboard versus standard of care in patients with Crohn's disease: study protocol for a randomised, controlled, multicentre, open-label study (the OPTIMIZE trial), BMJ Open 12 (2022).
[84] V.R. Figliuolo, R. Coutinho-Silva, C.M.L.M. Coutinho, Contribution of sulfate-reducing bacteria to homeostasis disruption during intestinal inflammation, Life Sci. 215 (2018) 145–151.
[85] D. Dordević, S. Jančíková, M. Vítězová, I. Kushkevych, Hydrogen sulfide toxicity in the gut environment: meta-analysis of sulfate-reducing and lactic acid bacteria in inflammatory processes, J. Adv. Res. 27 (2021) 55–69.
[86] J. Aresti Sanz, S. El Aidy, Microbiota and gut neuropeptides: a dual action of antimicrobial activity and neuroimmune response, Psychopharmacology (Berl). 236 (2019) 1597–1609.